Optical properties, surface composition and desorption of Stainless Steel (316L) studied from ambient temperature to 1000 K in vacuum

Cyprien Louis de Canonville, Marco Minissale, Francisco Romero-Lairado, Eric Salomon, Gregory Giacometti, Thierry Angot, Régis Bisson, Laurent Gallais

Optical properties and surface composition of Stainless Steel (316L) studied from ambient temperature to 1000 K.

Cyprien Louis de Canonville[1,2], Marco Minissale[2], Francisco Romero-Lairado[2], Eric Salomon[2], Gregory Giacometti[2], Thierry Angot[2], Régis Bisson[2], Laurent Gallais[1]

[1] Aix Marseille Univ, CNRS, Centrale Marseille, Institut Fresnel, France
[2] Aix Marseille Univ, CNRS, PIIM, France

E-mail: marco.minissale@amu-univ.fr, regis.bisson@amu-univ.fr, laurent.gallais@fresnel.fr

31 mars 2023

Abstract. Stainless steels are widely used as structural materials due to their excellent corrosion resistance and fabricability. In some applications, in nuclear fusion reactors for instance, these materials may be exposed to harsh conditions, including high heat flux and ion bombardment, which can significantly affect their surface properties and composition. In this work, we investigate the temperature-dependent evolution of the surface composition and optical properties (reflectivity, emissivity) of stainless steel 316L. X-ray photo-electron spectroscopy analyses, temperature programmed desorption and reflectivity measurements in the visible/near-infrared range were performed on polished samples from ambient temperature to 1000 K. It was found that around 750 K, the initial Fe/Cr surface abundance of 90/10 changes to 35/55, with Cr scavenging oxygen initially bound to Fe. In addition, Mn segregated at the surface and oxidized, while small amounts of metallic Ni segregated. Despite these modifications in surface composition, no significant change in reflectivity up to 900 K was observed. These results provide insight into the behavior of stainless steel under extreme conditions which is relevant for understanding its performance and durability in high-temperature applications.

Keywords: Stainless Steel, Optical Properties, Surface Composition, High Temperature, Annealing

1. Introduction

The optical properties (absorption, emissivity, reflectivity) of metal surfaces at high temperatures are crucial for numerous applications. Such applications include energy production in solar power plants with metallic reflectors or absorbers heated to temperatures of 700 K and higher [1], materials in fission nuclear reactors where

emissivity is a critical parameter to dissipate heat [2], plasma-facing components or first mirrors subjected to high thermal flux in fusion reactors [3], metallic parts of spacecrafts exposed to solar radiation or re-entry atmospheric conditions [4], and industrial processes such as laser welding, cutting or polishing. Among metals, stainless steel is a commonly employed structural material due to its good fabricability and corrosion resistance based on an oxide layer (Cr_2O_3, Mn_2O_3) that acts as a shell against corrosion. The composition also provides heat-resistant properties since it prevents oxidation: chromium reacts with oxygen to form a chromium oxide scale, which reduces oxygen diffusion into the material. The evolution of surface properties of SS316L at high temperature is the subject of many studies to investigate oxidation behavior [5, 6] or to develop thermal barrier coatings that can improve the corrosion resistance at high temperature [7, 8]. However, the topic of the optical properties of stainless steel is not extensively covered in the published literature, likely because it is not commonly used in optical applications. The optical properties of stainless steel are strongly affected by the roughness related to surface preparation, and they are also dependent on the surface composition of different grades of stainless steel. Karlson and Ribbing [9] have, for instance, compared different grades of stainless steel and found that the reflectance, in the UV to NIR spectral range, is primarily determined by the metallurgic phase: austenitic, ferritic or martensitic. Karlson and Ribbing's work serves as a foundation for studies of stainless steel, as it provides access to optical constants calculated by Kramers-Kronig analysis, which have been obtained at ambient temperature. Boydag [1] has studied the optical properties from ambient temperature to 500 K of steel surfaces (austenitic and ferritic steels) subjected to different chemical and mechanical surface treatments and has shown the influence of the surface preparations on the spectral selective properties, with significant changes related to oxidation.

In this study, we investigate the impact of high temperatures on the surface properties of stainless steel 316L (SS316L), which is a widely used material in the construction of ITER [10]. SS316L belongs to the austenitic family of stainless steels and consists primarily of iron, chromium (between 16–18%), nickel (10–12%), and molybdenum (2–3%), with small amounts (<1%) of carbon, silicon, phosphorus, and sulfur. The addition of molybdenum enhances its corrosion resistance compared to other stainless steel grades. Moreover, the low carbon content of SS316L makes it an ideal option for welding to ensure maximum corrosion resistance. Our study aims to analyze the effects of temperature on the surface roughness, composition, and optical properties of SS316L, which are likely to be modified under the harsh conditions to which the material will be exposed in ITER [11]. By investigating these effects, we gain useful insights for the development of materials for high-temperature applications.

2. Materials and Methods

2.1. Samples preparation

The materials used in this work were provided by GoodFellow with a specified content in mass fraction of 18% Chromium, 10% Nickel and 3% Molybdenum. 0.5 mm thick plates were cut into specimens with dimensions: $12.0 \times 12.0 \times 0.5\,mm^3$. They were delivered annealed tempered with a polished surface finish on both sides. The preparation process performed before conducting the experiments consists of a mechanical polishing procedure followed by cleaning. The polishing process is conducted with an automatic wheel grinder and polisher (ESCIL Saphir 520) and consists of several stages with different polishing pads and lubricants (alcohol and water-based). The automatic polishing machine allows for polishing up to five specimens simultaneously by controlling the force applied to each specimen (5 to 100 N), the polishing time, as well as the speed and direction of rotation of the plate (50 - 600 rpm). The samples are pre-coated with resin in order to facilitate the setting of the sample and to limit the edge effects, thus promoting uniformity of polishing on the surface. The details of the polishing procedure is given in Table 1

Table 1. The polishing procedure applied to the samples

Step	Polish. Disks	Suspension	Duration	Force	Speed	Lubricant
1	Felt P	Diamond 10 μm	1 min 30 s	30 N	150 rpm	LPS4
2	Felt B	Diamond 3 μm	1 min 30 s	30 N	150 rpm	LPS4
3	Felt V	1PS4A	1 min 30 s	30 N	150 rpm	LPS4
1	Felt FD1N	POM 8	1 min 30 s	25 N	120 rpm	LPS4

A mirror-like finish is obtained, with the surface properties characterized in the next section. The samples are cleaned in an ultrasonic bath for 10 minutes each, successively in acetone and ethanol solutions, before and after the polishing procedures.

2.2. Samples properties

The initial state of the samples was characterized prior to the temperature-dependent experiments. The surface topography was measured with an optical profilometer and an atomic force microscope to access different spatial scales and spatial frequencies. A commercial spectrophotometer was employed to measure the reflectivity in the visible and near-infrared range.

Optical profilometry was performed with a low coherence scanning interferometer (Zygo NewView 7300). A 10X Mirau objective with 0.3 numerical aperture providing a lateral resolution of $1.1\,\mu m$ in a field of view of $1.4 \times 1.0\,mm^2$ was employed. Stitching mode was applied to cover a few mm^2 of the sample surface, which corresponds to the probed area for our reflectivity measurements. This measurement gives access to the form or

waviness of the surface in the mm range and the roughness in the $10^{-3} - 10^{-1}\,mm^{-1}$ spatial frequency range. Measurements taken in the sample center (probed area in the experiments) are given in Figure 1 at different scales. The surface profile exhibits low-frequency (mm scale) deformations with $1\,\mu m$ amplitude. Such deviations from the desired planar form are caused by some inaccuracies in the polishing process, but they stay reasonable: such deviations correspond to one wavelength at $1\,\mu m$, the maximum wavelength of our study, which can be considered as a typical optical mirror grade.
Atomic Force Microscope measurements were performed on the polished sample with an NT-MDT Spectrum Instruments system. Measurement were done on a $30 \times 30\,\mu m^2$ surface in order to characterize the roughness. A measurement is given in Figure 1. The surface exhibits scratches related to the polishing process and a surface root mean square height (S_q) of 25 nm.

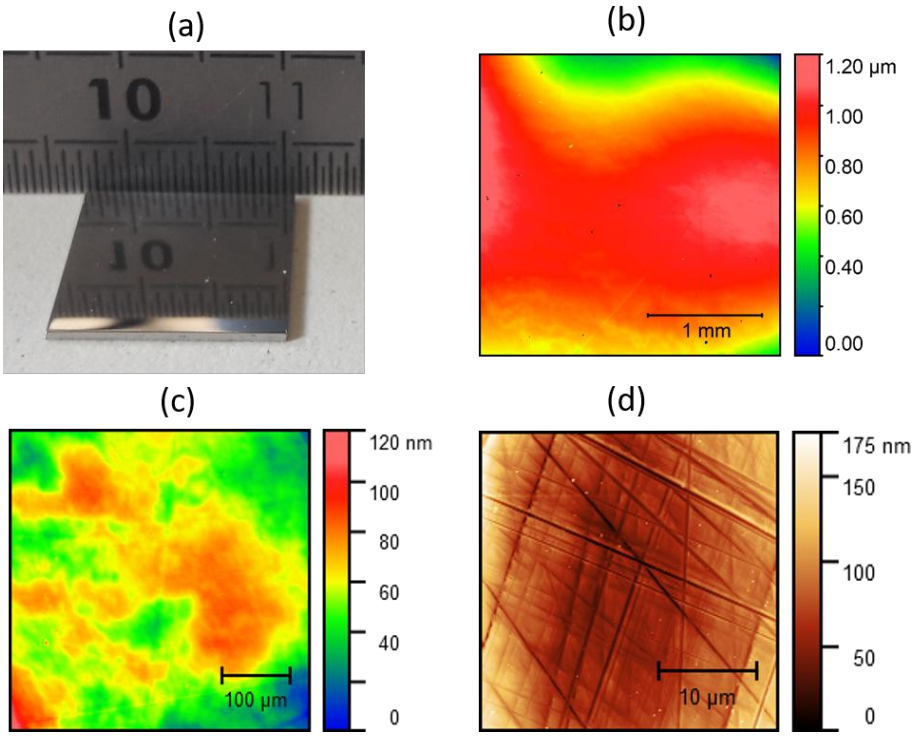

Figure 1. Surface topography of the polished samples. (a) Mirror finished of the $12 \times 12\,mm^2$ sample ; (b) and (c) Surface topographies obtained by Optical Profilometry ; (d) Surface topography obtained by Atomic Force Microscopy.

To characterize the optical properties of the samples, reflectivity measurements were performed using a Perkin Elmer Lambda 1050 spectrophotometer equipped with a Total Absolute Measurement System (TAMS) for absolute specular reflectance measurements. The spectrophotometer covered the range of 250-2500 nm with 5 nm intervals, and was operated in unpolarized mode at an 8 degrees angle of incidence. The reflectance spectrum of a polished and cleaned sample is presented in Figure 2.

The reflectance of the samples is found to increase monotonically with increasing

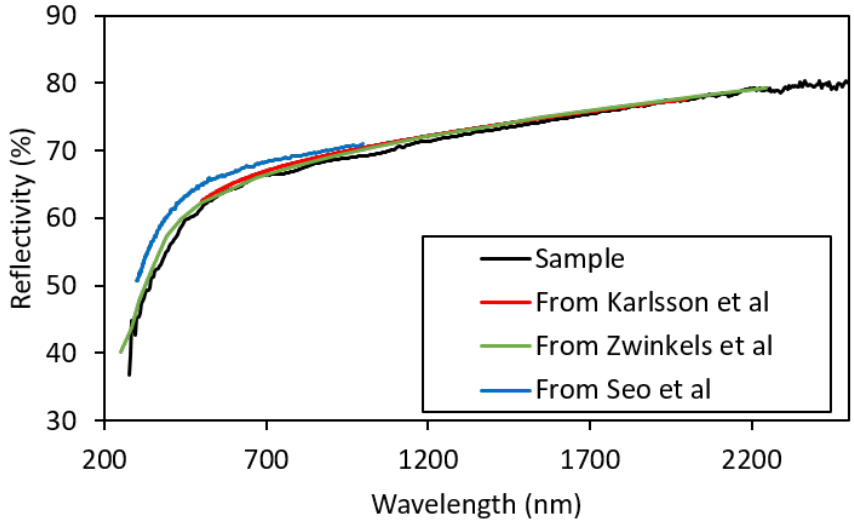

Figure 2. The specular reflectivity measured on one of the sample at 8 degrees of incidence, and its comparison to various published data [9, 12, 13].

wavelength from approximately 50 % at 250 nm to 80 % at 2500 nm. This behavior is typical of stainless steel, and the measured values are in good agreement with other reported data, as shown on the comparison with published data in Figure 2: the reflectivity calculated from the optical constants determined by Karlsson and Ribbing [9] on Avesta 832 mv alloy that has similar composition as SS316L and reflectivity measured by J.C. Zwinkels et al on SS304 [12], an alloy with a slightly different composition (304 contains a few percent more chromium and less nickel than 316L while molybdenum is present only in 316L). The reflectivity calculated with the refractive indices of 316L stainless steel determined by Seo et al. [13], with ellipsometry on polished samples, is also reported. The comparison shows a good match between different results reported in the literature, indicating that the composition among the samples has very little effect on the reflectance for one particular metallurgical phase, which is austenitic in this case. It is also noted that Karlsson and Ribbing [9] have systematically studied the optical properties of the natural oxides on stainless steels, Fe_2O_3 and Cr_2O_3, with the latter exhibiting a lower n value with a weaker dispersion than the former. The k values are also significantly lower in most of the visible spectrum.

3. Experimental

3.1. X-ray photoelectrons spectroscopy

X-ray Photoelectrons Spectroscopy (XPS) analyses were performed with an experimental setup composed of a high-intensity twin (Mg/Al) anode X-ray Source (provided by PREVAC) emitting at 1253.6 and 1486.6 eV respectively. The analyzed samples were placed in a movable sample holder inside a mu-metal ultra-high vacuum chamber with a base pressure of 1×10^{-10} mbar. Photoelectrons were detected via

a high-resolution electron energy analyzer (Scienta Omicron R3000). The analyzer was composed of a high transmission electron lens with an acceptance angle of 30 degrees and a 40 mm MCP detector, which was monitored by a FireWire CCD-Camera. The resolution of the XPS spectrometer, determined from the full-width at half maximum of the Ag 3d core levels of a clean Ag single crystal, was 0.9 eV [14]. The sample temperature was progressively varied from 300 to 950 K, and conducted XPS measurements by holding the sample at the desired temperature for about one hour.

3.2. Temperature programmed desorption

Temperature programmed desorption (TPD) was conducted in CAMITER [15], a UHV setup with a base pressure of 2×10^{-9} mbar. The sample was attached to a molybdenum sample holder, introduced in vacuum through a fast load-lock system and installed ontop of a radiative oven. After degassing for a couple of hours at 320 K, the sample was positionned 2 mm from the 2 mm aperture of a differentially pumped quadrupole mass spectrometer (Hiden 3F/PIC) with a line-of-sight to the sample surface thanks to a cross molecular beam ionization head. Thus, desorbed species from the sample enter directly in the mass spectrometer ion source. Then, the sample temperature was increased linearly at 1 K.s^{-1} up to 1000 K and the TPD from the sample was recorded in the mulitplexed mode of the mass spectrometer for the following species of interest: H_2O (m/z=18), O_2 (32), Cr (51.94), Mn (54.94), Fe (55.94), Ni (57.94), CrO (67.94) and Cr_2O_3 (151.87) as well as Mn, Fe and Ni oxides (not shown). Once the sample was cooled down to room temperature, a second TPD was realized on the same sample. Five samples have been measured and showed similar results and the results of one sample are presented here for which the above mentionned m/z species have been chosen with optimized counting statistics.

3.3. Visible to near infrared reflectivity

A home-made experimental setup was used to measure the evolution of the samples' reflectivity with temperature. It is based on the experimental configuration described in the work of Minissale et al [16] and is shown in Fig. 3.

The sample is placed in a vacuum chamber under a pressure of 10^{-8} mbar. It is held by an alumina custom-made sample holder. The sample was heated from the rear face (unpolished face) using a 200 W fibered 808 nm laser diode system (AMTRON, JENOPTIK). The temperature was measured with a monochromatic pyrometer (Sensortherm, Metis M3) operating in the 2-2.6 μm spectral range. The pyrometer has a 1 ms response time, a 0.6 mm spot size measurement, and can measure temperatures in the range of 350-1500 K. The pyrometer and laser head were positioned 30 cm away from the sample, targeting the sample through a BaF_2 viewport in the vacuum chamber. A temperature controller (Sensortherm, PID program controller Regulus RD) connected to the pyrometer and the laser is used to control the power of the heating laser as a function of the measured temperature of the sample, which

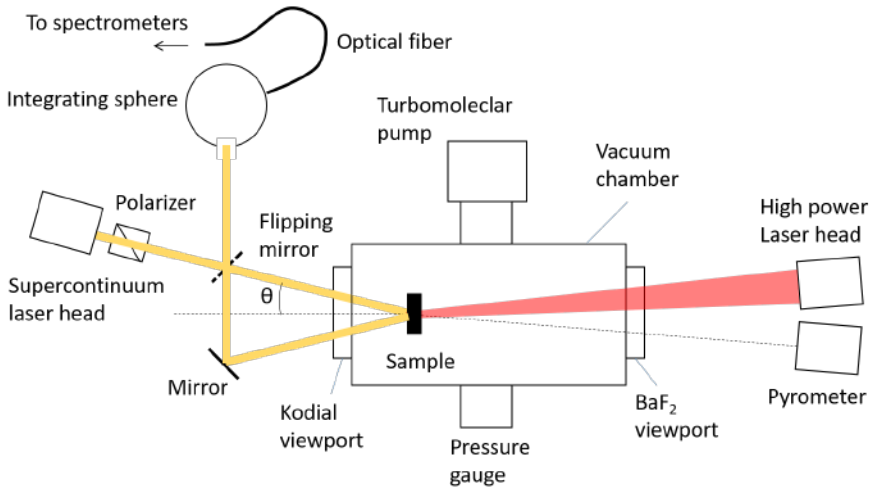

Figure 3. Shematic of the experimental configuration for temperature dependent reflectivity measurements.

ensures stable and well-controlled heating. The pyrometer measurement depends on the emissivity setting for the wavelength range being used. It was set to 0.2 after a calibration procedure involving a sample with a welded thermocouple. The laser beam has a quasi-Gaussian profile in the sample plane with a diameter of 3 mm, which is smaller than the sample lateral dimensions. As a result, spatial thermal gradients were generated on the surface and in the depth of the sample, that were estimated with thermal simulations performed with a Finite Element Model (COMSOL Multiphysics software) with thermal parameters extracted from the ITER database. These simulations evidence that because of the relativelly low thermal conductivity of SS316L and spatial distribution of the beam, the temperature in the area of interest is not homogeneous. Figure 4 shows an example of a laser-heated sample, along with the results of a thermal simulation that shows temperature gradients on the surface of interest at 1300 K. Since optical measurements probe the surface at the center of a 2 mm diameter area, the temperature inhomogeneity should be associated with an error bar of $\pm 5\%$.

Spectrophotometric measurements are taken on the front side of the sample (opposite to the heating), using a supercontinuum white light source (SM-30400, Leukos). The source emitted 100 mW in the 400-2400 nm range, was collimated, and directed towards the sample. The beam was polarized with a linear polarizer (LPVIS100-MP2, Torlabs), and the angle of incidence adjusted in the range of 10-55 degrees. The beam has a diameter of 1.5 mm on the sample surface and the reflectivity is thus probed within this diameter. The reflected beam was directed to an integrating sphere (AvaSphere-80, Avantes) made of Spectralon using a silver mirror. It has to be noted that the beam passes through the vacuumm window twice (before and after reflection on the sample), as shown on figure 3 that depicts the configuration. Two fiber optic spectrometers (ULS2048L, Avantes and AvaSpec-NIR256/512-2.5-HSC-EVO, Avantes)

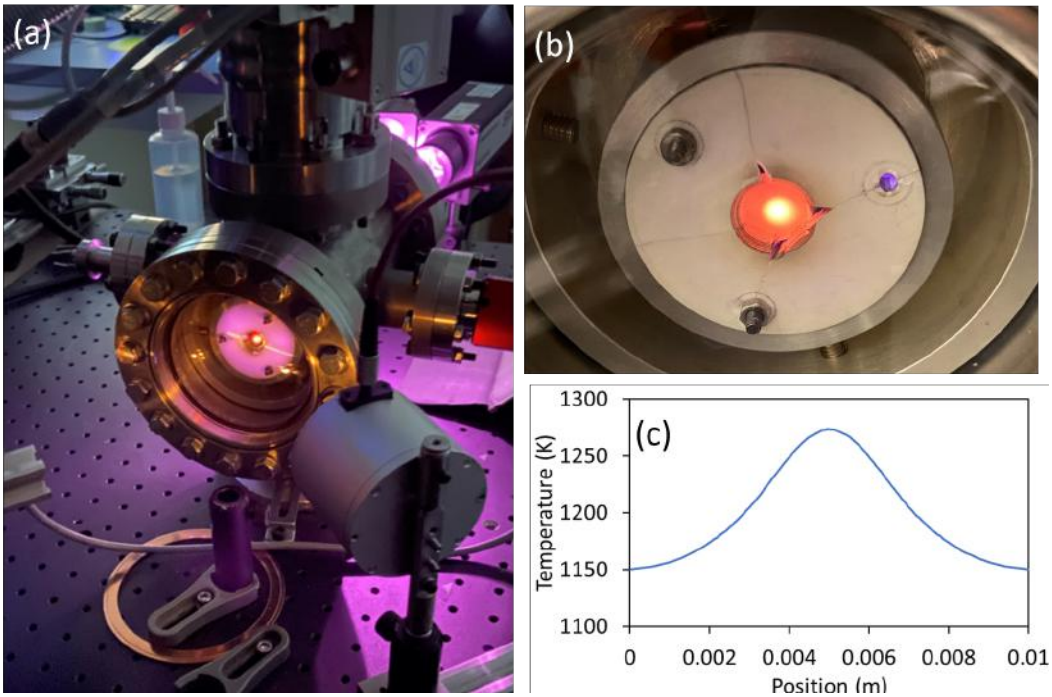

Figure 4. Laser heating of a SS316L sample. (a) An overview of the experimental setup during a laser heating sequence. (b) View of the sample and sample holder in the vacuum chamber, from opposite side of laser heating. The thermal gradients are evidenced by the thermal radiation and associated color gradients. (c) Results of a thermal simulation with a plot of temperature on the surface of the sample, on opposite side of laser heating.

are connected to the integrating sphere to measure the spectrum in the 500-1100 nm and 1000-2000 nm ranges, respectively. The measurement protocol, described in reference [16], involves taking a reference measurement on a silver mirror (flipping mirror in the figure) and determining the vacuum window transmission in order to obtain the reflectivity of the sample of interest.

4. Results and discussion

4.1. Surface composition as a function of temperature

In this section we present the temperature dependence of the elemental surface composition of the samples performed using XPS as well as the temperature dependence of the desorbing species using Temperature Programmed Desorption (TPD).

The XPS analysis was performed on the sample held at different temperatures (300, 500, 650, 750, 850 and 950 K) for more than 30 minutes. The results of the XPS analysis are presented in Figure 5. Four different regions were recorded to characterize the evolution of the surface composition of the main elements of the SS316L: (a) Fe 2p between 725-695 eV, (b) Cr 2p between 600-565 eV, (c) Ni 2p between the 885-845 eV, and (d) Mn 2p between 665-630 eV. Moreover, the C 1s and O 1s regions were

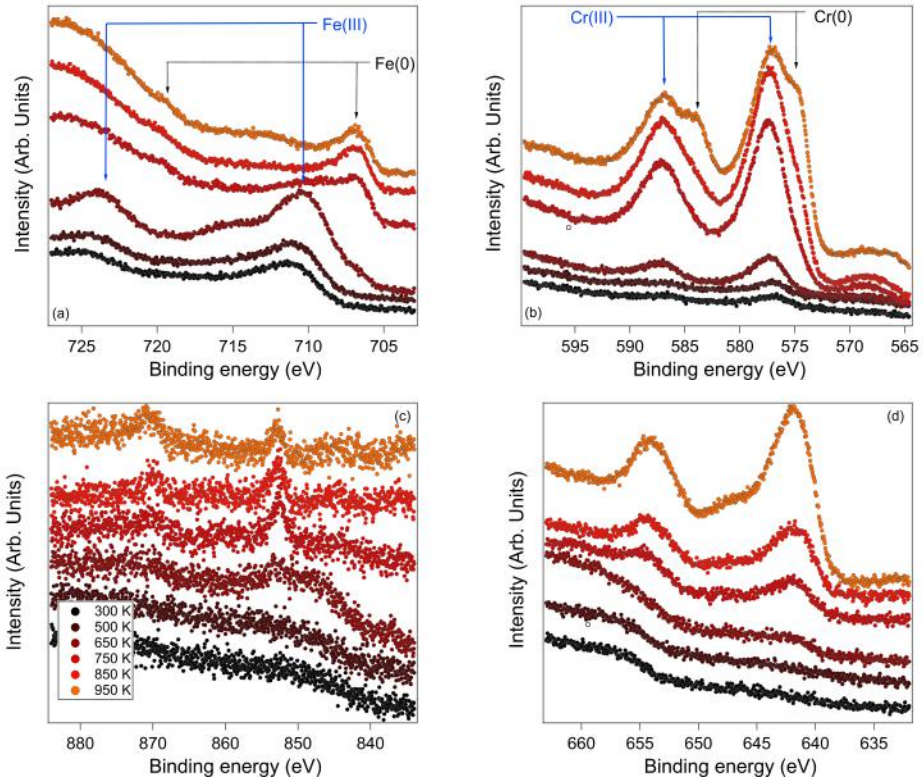

Figure 5. XPS spectra recorded on four different energy regions on a SS316L hold at different temperatures: a) evolution of Fe 2p core level of Fe(0) (metal) and Fe(III) (oxide); b) evolution of Cr 2p core level of Cr(0) (metal) and Cr(III) (oxide); c) evolution of Ni 2p core level for Ni(0) (metal); d) evolution of Mn 2p core level of Mn oxides.

systematically recorded (not shown in Figure 5).

In the case of the as-introduced sample at RT only Fe and Cr oxides are clearly detectable: 1) Fe $2p^{1/2}$ and Fe $2p^{3/2}$ were detected at 711 and 724 eV respectively and indicate the presence of of Fe(III) (Fe_2O_3) [17], while Cr $2p^{1/2}$ and Cr $2p^{3/2}$ of Cr(III) (Cr_2O_3) are detected at 587.1 and 577.2 eV, respectively, in agreement with [18]. One can note that at 750 K the iron oxides are much less visible and Fe 2p peaks are shifted to lower binding energy (around 4 eV) assigned to Fe(0). In all the cases the FWHM of peaks is 1.85±0.10 eV for metal peaks (e.g. Fe(0)), while it is around 4 eV in the case of oxides probably due to the coexistence of different oxidation states. The iron de-oxygenation is observed in XPS from 650 K, at the same time than the increase of the broad peak centered at 528 eV [19] that can be assigned to the LMV Auger peak of chromium. At 650 K, an increase of chromium oxide was observed with XPS (Figure 5b). Starting at 850 K, Cr(0) starts to be visible (584.6 and 574.2 eV). For temperature $\geq$ 750 K, Ni and Mn segregation at the surface was observed. Ni is detected at 869.8 and 852.6 eV [20] and it is assigned to Ni in its metallic form (Ni(0)). Ni intensity is rather constant up to 1100 K. Mn peaks are centered at 654.2 and 642 eV and can be assigned to Mn_xO_y [21, 22]. Using the photoionization cross-sections of the different

core levels at 1253.6 eV, the surface abundance for each temperature was estimated, which are presented in Figure 6.

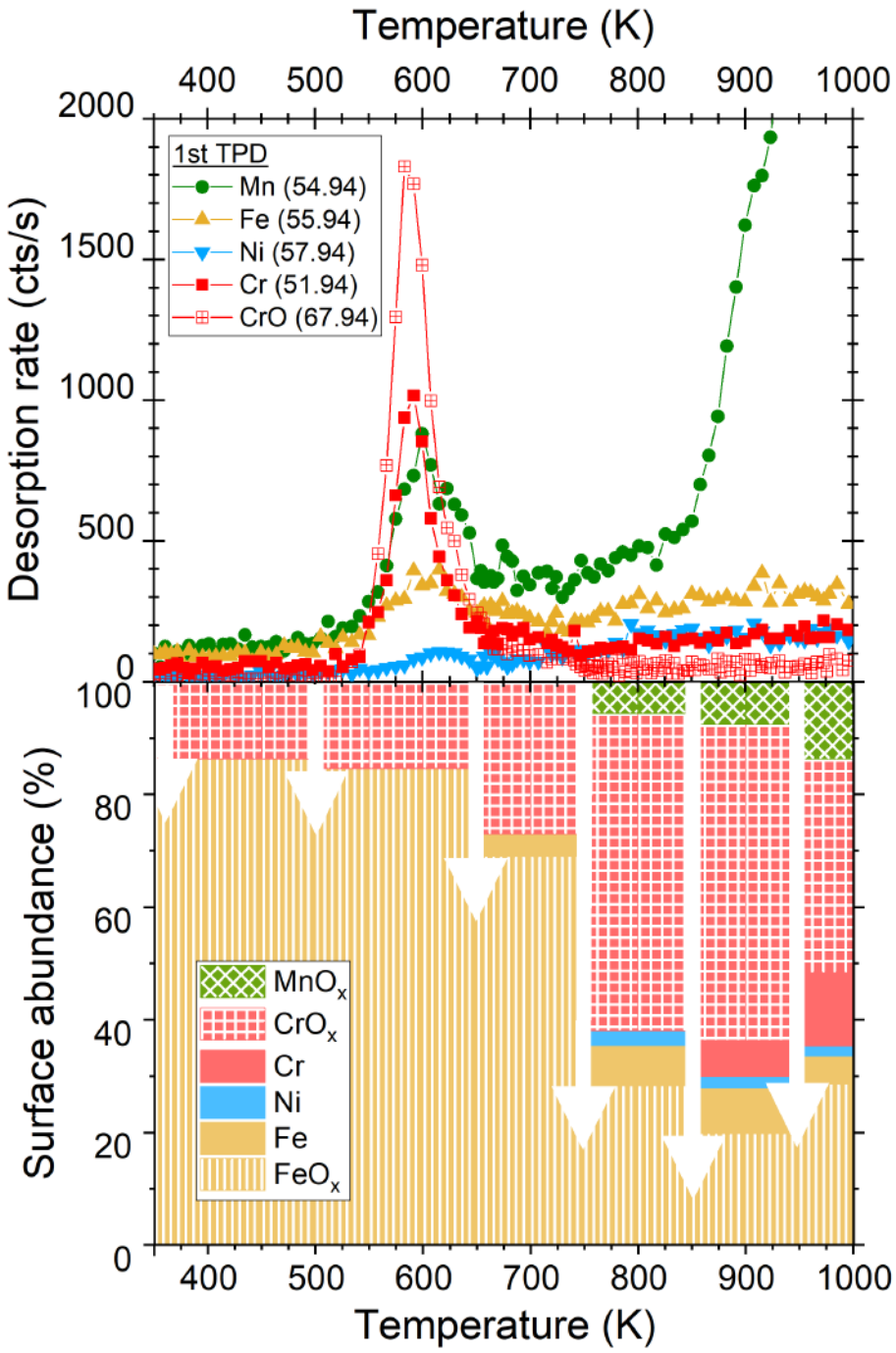

Figure 6. Top: TPD of SS316L upon its first annealing to 1000 K. The mass/charge ratio of desorbing elements is shown in parenthesis. Bottom: Evolution of the surface elemental abundance from the XPS analysis. The white arrows indicate at which moment of the TPD the annealing was interrupted to perform the XPS analysis.

The temperature programmed desorption of SS316L, also shown in Figure 6, can be separated in two steps. The first step occurs in the 550 K and 650 K range where

desorption of Cr and CrO species dominates, with smaller desorption peaks for the other metals (Mn, Fe and Ni). Note that CrO is the only oxide detected in the gas phase. We suggest that CrO desorption is a signature of the formation of CrO_x surface oxide, which surface abundance increases while iron oxide is depleted as shown by XPS. Since desorbing of FeO_x species was not observed, we propose that surface CrO_x grows by scavenging the oxygen of FeO_x, leading to the desorption of Fe atoms in TPD and the appearance of metallic Fe in XPS. High oxydation states of CrO_x oxides maybe unstable and could decompose at the surface leading to the desorption of CrO species and O_2 molecules (also detected as a desorption peak in the 550 - 650 K range, not shown). The second step of the desorption is seen above 750 K where the desorption rate of all four metals is increasing steadily. As these metal elements desorb in larger extent in TPD, one observed the appearance of all metal in XPS: Mn oxides and Ni appear at the surface at 750 K, while CrO is reduced to Cr at 850 K. Note that an important increase of Mn desorption is observed at 900 K, together with a further increase of its XPS surface oxide abundance at 950K.

When a second TPD was realized on the SS316L sample, after being cooled at room temperature, the occurence of the first step desorption in the 550 - 650 K range was not observed. Only the steadily increasing desorption of metal elements is observed above 750 K. In summary, XPS and TPD data show that the surface of SS316L is evolving in two steps. The first evolution step occurs around 600 K and is irreversible: it leads to the partial reduction of Fe and the growth of a chromium oxide. The second evolution step occurs above 750 K, where all elements are seen to desorb and a complex surface composition is obtained mixing Mn, Cr, Fe, Ni and some of their oxides.

4.2. Temperature dependent reflectivity measurements

The temperature-dependent reflectivity of the samples was measured at an angle of incidence of 45^o and in P polarization. The spectral range of measurement was restricted to 500-1000 nm due to limitations of the supercontinuum source, specifically insufficient power to overcome thermal radiation signal in the infrared and instabilities in the short wavelength range. Nevertheless, this restricted band is of great interest for observing potential evolution of optical properties with temperature since it corresponds to the range with the largest variations of reflectivity (see Figure 2). It should be noted that a high power laser (200 W) operating at 805 nm was used to heat the sample, and the reflectivity measurement in the 785-820 nm range is quite inaccurate. The instrument is less accurate than the commercial spectrophotometer described in section 2.2, and an accuracy of $\pm 1\%$ on the absolute reflectance was estimated. Figure 7 displays the measured reflectance on two different samples and their comparison to the theoretical reflectance calculated from the optical constants of stainless steel determined by Karlsson and Ribbing [9] labeled as 'reference' in the figure. The measured reflectivity is slightly below this reference value, which was also observed at normal incidence (see Figure 2).

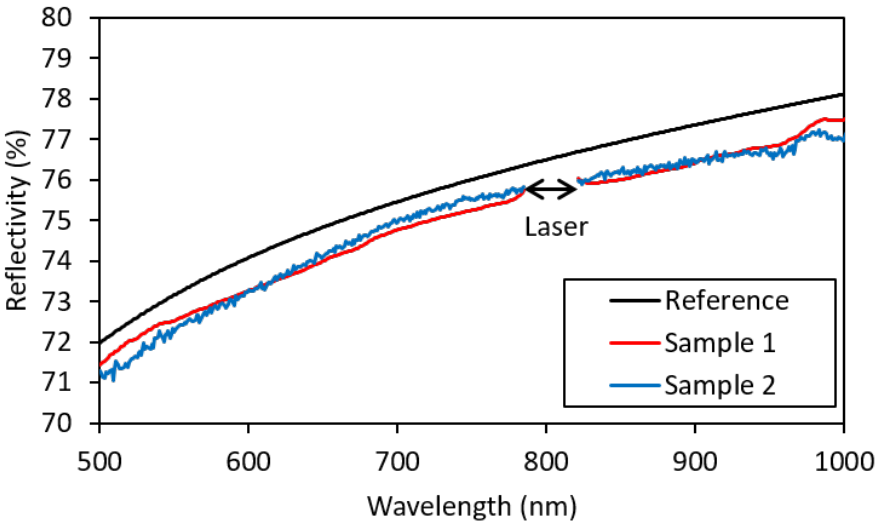

Figure 7. Reflectivity of two SS316L samples measured at an angle of incidence of 45^o and in P polarization at room temperature, on the experiment described in Figure 3. The experimental results are compared to the theoretical reflectivity calculated from the optical constants of stainless steel determined by Karlsson and Ribbing [9]. The arrow corresponds to the spectral bandwith of the laser source.

The samples were subjected to a series of successive heating ramps, as described in Figure 8, with the baseline temperature set to 423 K close to the minimum temperature that can be measured with our pyrometer. The temperature was then linearly increased in 450 s to successive target temperatures of 673 K, 873 K or 1073 K. The temperature was then ramped down to the baseline temperature, and the process was repeated a second time to check for repeatability and discriminate between possible reversible or irreversible processes. Higher temperatures were also explored, but above 1100 K, the thermal radiation from the sample was a limitation for acquiring the reflectivity spectrum in our configuration. A supercontinuum source with higher power would be required for measurements at higher temperatures. Reflectivity spectra were continuously acquired during the heating and cooling sequences, approximately every 2 seconds.

Figure 9 describes the results obtained on a sample heated to 673 K using the sequence outlined in Figure 8. Our findings indicate that no significant changes were observed in the reflectivity curve within the error margin of the instrument. Furthermore, the results were inconsistent when compared with results obtained from several other samples. As a result, it can be concluded that no notable alterations in optical properties under these heating conditions can be observed.

Figure 10 shows the results obtained on a sample heated to 873 K using the previously described sequence. A slight evolution of within $1-2\%$ from the initial reflectivity (1) is evidenced after the first heating (2), which has also been observed on several samples. From the XPS and TPD data described above, we propose that the change of chemical composition at the surface is the cause: Fe, initially 90% abundant

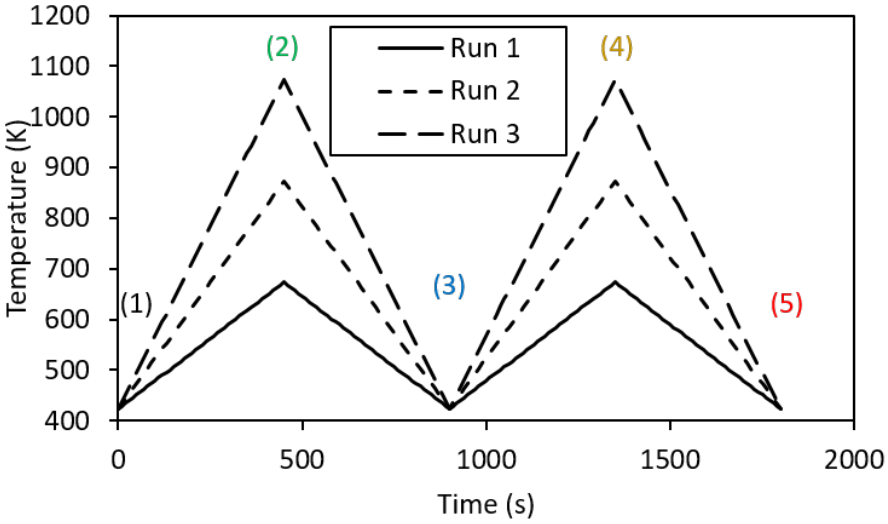

Figure 8. The heating sequence applied to the samples. The numbers in brackets correspond to the time position of the different reflectivity measurements given in the next figures.

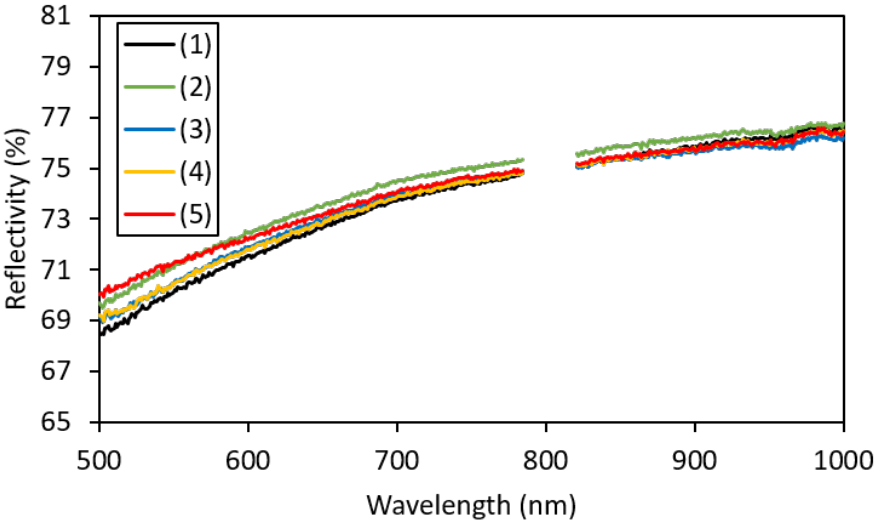

Figure 9. Reflectivity measurements at different time of the heating sequence. (1) 423 K, starting ot the first heating ramp ; (2) 673 K, end ot the first heating ramp ; (3) 423 K, end ot the first cooling ramp and starting of the second heating ramp ; (4) 673 K, end ot the second heating ramp ; (5) 423 K, end ot the second cooling ramp.

at the surface, drops to less than 30% surface abundance for heating above 750 K. This effect stabilizes after cooling down (3), and no further evolution is observed after the second heating ramp (4) and (5). Based on these results, it can be concluded that the observed modifications of composition with temperature have minor effect on the optical properties of SS316L.

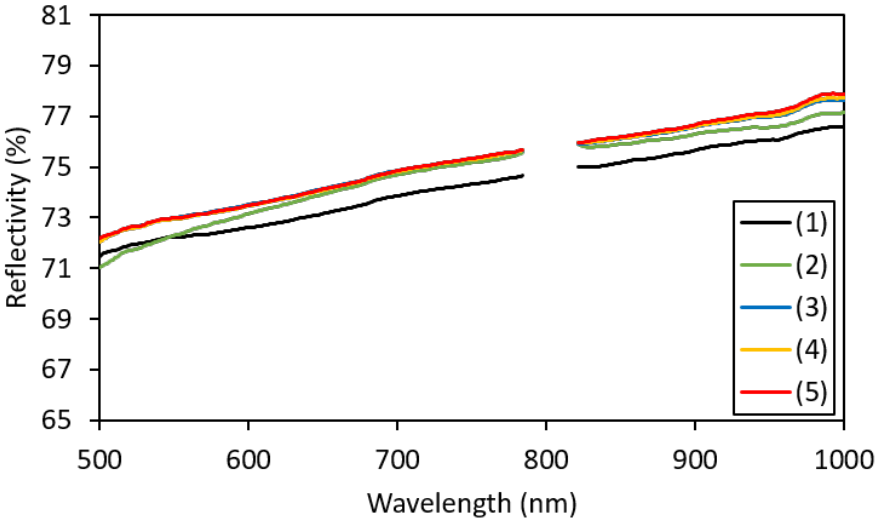

Figure 10. Reflectivity measurements at different time of the heating sequence. (1) 423 K, starting ot the first heating ramp ; (2) 873 K, end ot the first heating ramp ; (3) 423 K, end ot the first cooling ramp and starting of the second heating ramp ; (4) 873 K, end ot the second heating ramp ; (5) 423 K, end ot the second cooling ramp..

5. Conclusions

This study presents temperature-dependent X-Ray Electron Spectroscopy analyses, temperature programmed desorption data and reflectivity measurements in the visible/near-infrared range on polished SS316L samples in a vacuum environment. Our results show that below 750 K, there is a slight modification of the surface composition with a change in the initial Fe/Cr abundance from 88/12 to 73/27 while it does not induce significant reflectivity modification. However, above 750 K, a drastic evolution of the surface composition was observed, with a change in the initial Fe/Cr abundance to 35/50 and the appearance of Ni and MnO_x surface species. Combining XPS and TPD measurements, it is suggested that Cr scavenges the oxygen initially bound to Fe, while Mn segregates at the surface and oxidizes. Additionally, a small amount of metallic Ni segregates at the surface. Despite these modifications of the surface composition, a tenuous modification of the reflectivity around 900 K was observed. A possible explanation could be that the change in surface composition occurs on a thickness smaller than the light penetration depth of approximately 10 nm in the visible range.

Future studies could focus on extending these experiments to higher temperatures, or investigating other types of stainless steel samples to further understand the effects of temperature on their surface properties and optical behavior. Additionally, combining the surface analysis techniques with other analytical tools, such as atomic force microscopy, X ray diffraction, or Raman spectroscopy, could provide more detailed information on the physical and chemical changes occurring at the surface of the material.

Funding

The project leading to this publication has received funding from the Excellence Initiative of Aix-Marseille University—A*Midex, a French 'Investissements d'Avenir' programme as well as from the ANR under Grant ANR-18-CE05-0012.

References

[1] F.S. Boydağ. The optical properties of some steel surfaces with different surface preparations for high temperature use. *Solar Energy Materials*, 13(3):185–195, 1986.

[2] Tristan S. Hunnewell, Kyle L. Walton, Sangita Sharma, Tushar K. Ghosh, Robert V. Tompson, Dabir S. Viswanath, and Sudarshan K. Loyalka. Total hemispherical emissivity of ss 316l with simulated very high temperature reactor surface conditions. *Nuclear Technology*, 198(3):293–305, 2017.

[3] L. Marot, G. De Temmerman, P. Oelhafen, G. Covarel, and A. Litnovsky. Rhodium coated mirrors deposited by magnetron sputtering for fusion applications. *Review of Scientific Instruments*, 78(10):103507, 2007.

[4] E. Brodu, M. Balat-Pichelin, J.-L. Sans, and J.C. Kasper. Evolution of the emissivity of tungsten at high temperature with and without proton bombardment. *Acta Materialia*, 84:305–316, 2015.

[5] H. Buscail, S. El Messki, F. Riffard, S. Perrier, R. Cueff, E. Caudron, and C. Issartel. Characterization of the oxides formed at 1000°c on the aisi 316l stainless steel—role of molybdenum. *Materials Chemistry and Physics*, 111(2):491–496, 2008.

[6] Xi Huang, Kai Xiao, Xiaodong Fang, Zicheng Xiong, Lihua Wei, Pengcheng Zhu, and Xiaoyan Li. Oxidation behavior of 316l austenitic stainless steel in high temperature air with long-term exposure. *Materials Research Express*, 7(6):066517, 2020.

[7] A.F. Yetim, H. Tekdir, K. Turalioglu, M. Taftali, and T. Yetim. Tribological behavior of plasma-sprayed yttria-stabilized zirconia thermal barrier coatings on 316l stainless steel under high-temperature conditions. *Materials Letters*, 336:133873, 2023.

[8] T Yetim, H Tekdir, M Taftalı, K Turalıoğlu, and A F Yetim. Synthesis and characterisation of single and duplex zno/tio2 ceramic films on additively manufactured bimetallic material of 316l stainless steel and ti6al4v. *Surface Topography: Metrology and Properties*, 11(2):024005, 2023.

[9] Björn Karlsson and Carl G. Ribbing. Optical constants and spectral selectivity of stainless steel and its oxides. *Journal of Applied Physics*, 53(9):6340–6346, 1982.

[10] Hee-Jin Shim, Sawoong Kim, ByeongIl Park, Duck-Hoi Kim, and Volker Johansson. Fabrication and characteristic of the 316l(n)-ig forged block and rolled plate for application to iter blanket shield block. *Fusion Engineering and Design*, 156:111738, 2020.

[11] N.S. Klimov, J. Linke, R.A. Pitts, A.M. Zhitlukhin, D.V. Kovalenko, V.L. Podkovyrov, V.A. Barsuk, C. Thomser, G. Pintsuk, B.N. Bazylev, R.N. Giniyatulin, V.P. Budaev, and L.N. Khimchenko. Stainless steel performance under iter-relevant mitigated disruption photonic heat loads. *Journal of Nuclear Materials*, 438:S241–S245, 2013. Proceedings of the 20th International Conference on Plasma-Surface Interactions in Controlled Fusion Devices.

[12] Joanne C. Zwinkels, M. Noël, and C. X. Dodd. Procedures and standards for accurate spectrophotometric measurements of specular reflectance. *Appl. Opt.*, 33(34):7933–7944, Dec 1994.

[13] Minseok Seo, Jeeyoung Lee, and Myeongkyu Lee. Grating-coupled surface plasmon resonance on bulk stainless steel. *Opt. Express*, 25(22):26939–26949, Oct 2017.

[14] S. Salomon, M. Minissale, F. Romero Lairado, P. Coussan, S. Rousselot-Pailley, F. Dulieu, and T. Angot. Pyrene Adsorption on a Ag(111) Surface. . *Journal of Physical Chemistry C*, 125:11166–11174, February 2021.

[15] F. Ghiorghiu, T. Aissou, M. Minissale, T. Angot, G. De Temmerman, and R. Bisson. Nitrogen retention and ammonia production on tungsten. *Nuclear Fusion*, 61:126067, 2021.

[16] Marco Minissale, Cedric Pardanaud, Régis Bisson, and Laurent Gallais. The temperature dependence of optical properties of tungsten in the visible and near-infrared domains: an experimental and theoretical study. *Journal of Physics D: Applied Physics*, 50(45):455601, oct 2017.

[17] Hidetaka Konno and Masaichi Nagayama. X-ray photoelectron spectra of hexavalent iron. *Journal of Electron Spectroscopy and Related Phenomena*, 18(3):341–343, 1980.

[18] S. Mischler, H. J. Mathieu, and D. Landolt. Investigation of a passive film on an iron-chromium alloy by aes and xps. *Surface and Interface Analysis*, 11(4):182–188, 1988.

[19] I. Grohmann, E. Kemnitz, A. Lippitz, and W. E. S. Unger. Curve fitting of cr 2p photoelectron spectra of cr2o3 and crf3. *Surface and Interface Analysis*, 23(13):887–891, 1995.

[20] A. M. Venezia, R. Bertoncello, and G. Deganello. X-ray photoelectron spectroscopy investigation of pumice-supported nickel catalysts. *Surface and Interface Analysis*, 23(4):239–247, 1995.

[21] Hugo F. Franzen, Mirtha X. Umaña, J.R. McCreary, and R.J. Thorn. Xps spectra of some transition metal and alkaline earth monochalcogenides. *Journal of Solid State Chemistry*, 18(4):363–368, 1976.

[22] G.C. Allen, S.J. Harris, J.A. Jutson, and J.M. Dyke. A study of a number of mixed transition metal oxide spinels using x-ray photoelectron spectroscopy. *Applied Surface Science*, 37(1):111–134, 1989.